Ultrasonics Sonochemistry 109 (2024) 107018

Contents lists available at ScienceDirect

Ultrasonics Sonochemistry

journal homepage: www.elsevier.com/locate/ultson

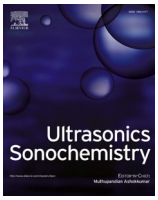

Revolutionizing wild silk fibers: Ultrasound enhances structure, properties, and regenerability of protein biomaterials in ionic liquids

Xincheng Zhuang [a,b], Haomiao Zhu [b], Fang Wang [a,b,*], Xiao Hu [c,d,*]

[a] Center of Analysis and Testing, Nanjing Normal University, Nanjing 210023, China
[b] School of Chemistry and Materials Science, Nanjing Normal University, Nanjing 210023, China
[c] Department of Physics and Astronomy, Rowan University, Glassboro, NJ 08028, USA
[d] Department of Biological and Biomedical Sciences, Rowan University, Glassboro, NJ 08028, USA

ARTICLE INFO

Keywords:
Ultrasound
Ionic liquid
Wild tussah silk
Spray spinning technology

ABSTRACT

Ultrasound-assisted regulation of biomaterial properties has attracted increasing attention due to the unique reaction conditions induced by ultrasound cavitation. In this study, we explored the fabrication of wild tussah silk nanofiber membranes via ultrasound spray spinning from an ionic liquid system, characterized by scanning electron microscopy (SEM), Fourier transform infrared spectroscopy (FTIR), X-ray powder diffraction (XRD), differential scanning calorimetry (DSC), thermogravimetric analysis (TGA), atomic force microscopy (AFM), water contact angle, cytocompatibility tests, and enzymatic degradation studies. We investigated the effects of ultrasound propagation in an ionic liquid on the morphology, structure, thermal and mechanical properties, surface hydrophilicity, biocompatibility, and biodegradability of the fabricated fibers. The results showed that as ultrasound treatment time increased from 0 to 60 min, the regenerated silk fiber diameter decreased by 0.97 μm and surface area increased by 30.44 μm^2, enhancing the fiber surface smoothness and uniformity. Ultrasound also promoted the rearrangement of protein molecular chains and transformation of disordered protein structures into β-sheets, increasing the β-sheet content to 54.32 %, which significantly improved the materials' thermal stability (with decomposition temperatures rising to 256.38 °C) and mechanical properties (elastic modulus reaching 0.75 GPa). In addition, hydrophilicity, cytocompatibility, and biodegradability of the fiber membranes all improved with longer ultrasound exposure, highlighting the potential of ultrasound technology in advancing the properties of natural biopolymers for applications in sustainable materials science and tissue regeneration.

1. Introduction

In the past decades, the extensive use of non-biodegradable and petroleum-based materials has caused significant negative impacts on the environment [1,2]. Considering the rising oil prices in recent years and national efforts to develop renewable resources, it is likely that fossil resources such as coal, oil, and their derivatives will become scarce, exacerbating the impacts of the energy crisis [3]. This scenario has spurred growing demand for renewable and environmentally friendly alternatives, steering research toward improving the biodegradability and eco-friendliness of polymer materials [4].

Natural polymeric materials, primarily derived from renewable or biological sources such as plants and animals, are abundantly available, have low production costs, and exhibit superior biodegradability and biocompatibility, making them more attractive than petroleum-based materials [5–8]. These materials are particularly advantageous in the field of bioengineering due to their commercial viability and high compatibility with human tissues [8,9]. Tussah silk, a common natural polymer produced by wild tussah larvae, consists of two parallel flat monofilaments primarily composed of fibroin and silk sericin glue [10–12]. This silk can be processed into various structural and morphological forms like nanofibers, films, and gels through degumming and dissolution steps [10,13,14], and can be combined with other materials [12]. Compared with *Bombyx mori* silk fibroin from domestic silkworms, tussah silk proteins offer similar advantages, including good air permeability, moisture absorption, biocompatibility, ease of processing, and degradability [15]. Additionally, due to their superior heat and corrosion resistance, mechanical properties, and cell adhesion

* Corresponding authors at: Center of Analysis and Testing, Nanjing Normal University, Nanjing 210023, China.
E-mail addresses: wangfang@njnu.edu.cn (F. Wang), hu@rowan.edu (X. Hu).

https://doi.org/10.1016/j.ultsonch.2024.107018
Received 10 May 2024; Received in revised form 17 July 2024; Accepted 5 August 2024
Available online 8 August 2024

capabilities, tussah silk proteins are more promising biomaterials for tissue regeneration [15–17].

However, tussah silk fibroin protein (TSF) is resistant to dissolution in common acids, alkalis, and organic solvents due to its acid and alkali resistance [18]. While high-concentration salt solutions (LiBr-H_2O, $CaCl_2$-C_2H_5O-H_2O, LiSCN aqueous solution) and chlorinated solutions (trifluoroacetic acid, hexafluoroisopropanol) can effectively dissolve silk at the molecular level [12,18–20], these solvents pose significant health and environmental risks and are difficult to recycle. Ionic liquids, a new class of green solvents made up of cations and anions with flexible conformations [18,21,22], offer a safer alternative. They solve the issues of toxicity and environmental harm associated with conventional solvents due to their excellent solubility, thermal stability, low volatility, and low toxicity, while also preserving the protein structure and maintaining molecular weight [20,21,23,24]. Therefore, ionic liquids were employed to dissolve tussah silk in this study.

Ultrasound treatment, a technology known for its high efficiency, ease of operation, and controllability [25,26], uses dense, alternating longitudinal waves that interact mechanically, cavitationally, and thermally with materials as they propagate, altering the polymer's structure and influencing its physical and chemical properties [26,27]. For instance, Cho et al. [28] successfully prepared water-soluble chitin for wound healing by controlling the degree of deacetylation and molecular weight through ultrasound treatment. Aluigi et al. [29] recovered keratin material from wool fiber waste using enzyme-ultrasound treatment. Additionally, varying ultrasound conditions can differentially affect the structure and properties of materials. For example, moderately increasing ultrasonic power amplitude can break or recombine the molecular chains of biological macromolecules (such as proteins and polysaccharides) and change their molecular structures [26,27]. However, if the ultrasonic duration is too long, it may cause thermal effects, leading to material denaturation or degradation and affecting its mechanical properties [26]. Our research [30] demonstrated that increasing the ultrasound time from 30 to 180 min in a formic acid/$CaCl_2$ solvent system increased the β-sheets content of soy protein/silk protein composites from 37.8 % to 50.2 %, significantly enhancing their mechanical properties and hydrophilicity. Wang et al. [31] also found that ultrasound-assisted wood dyeing increased dye absorption from 5 % to 25.5 % by boosting ultrasound power from 0 to 200 W, as the high-power ultrasound enhanced the permeability of the wood and activated the dye molecules, allowing more dye to penetrate the wood.

Utilizing a simple and effective ultrasound method to regulate the structure and properties of tussah silk materials is of great practical significance for developing advanced materials. In addition, exploring the interaction of ultrasound waves in ionic liquids as opposed to regular organic solvents also opens fascinating avenues for research, particularly in how these mediums influence the final structure and properties of silk materials. The unique ionic environment may enhance ultrasound's effects on molecular alignment and crystallinity changes compared to organic solvents, potentially leading to fibers with distinct physical and chemical characteristics.

In this study, the ionic liquid 1-Allyl-3-methylimidazolium chloride (AMIMCl) was used as the solvent to smoothly dissolve tussah silk proteins, selected for its superior ability to disrupt hydrogen bonds within the silk fibroin structure, facilitating rapid and complete dissolution. Uniform tussah silk nanofiber membranes were prepared using ultrasound treatment combined with solution spray spinning techniques. The effects of different ultrasound treatment durations on the structural transformation and physicochemical properties of tussah silk materials were systematically investigated. Techniques such as scanning electron microscopy (SEM), Fourier transform infrared spectroscopy (FTIR), and X-ray powder diffraction (XRD) were employed to assess the morphology and secondary structure, while differential scanning calorimetry (DSC), thermogravimetric analysis (TGA), and atomic force microscopy (AFM) characterized the thermal and mechanical properties. Additionally, the surface hydrophilicity, cytocompatibility, and biodegradability of the tussah silk materials were evaluated through water contact angle measurements, cytotoxicity tests, and enzymatic degradation experiments. This comprehensive approach not only furthers the development of advanced, controllable tussah silk materials using green solvents and physical methods but also can promote their application in biomedical and tissue engineering fields, contributing to the achievement of sustainable development goals (SDGs) due to the green, simple, and reliable nature of this fabrication method. Specifically, it positively impacts the realization of "Affordable and Clean Energy" (SDG-7) and "Responsible Consumption and Production" (SDG-12). Table 1 summarizes several research examples dedicated to advancing sustainable development goals.

2. Experiments

2.1. Materials and instruments

Raw materials and equipment were obtained from the following sources: wild silkworm cocoons (Tussash, July Trading Co., Ltd., Liaoning, China); 1-allyl-3-methylimidazolium chloride (AMIMCl, Shanghai Chengjie Chemical Co., Ltd., Shanghai, China); oil bath pan (DF-101S, Shanghai Xiniu Leibo Instrument Co., Ltd., Shanghai, China); ultrasonic equipment (YMNL-950Y, Nanjing Emmanuel Instrument Equipment Co., Ltd., Nanjing, China); spinning device (DQE750-24L, Jiangsu Dongcheng Electric Tools Co., Ltd., Nantong, China); oven (DHG-9030A, Wuxi Mareit Technology Co., Ltd., Wuxi, China).

2.2. Sample preparation

Initially, the tussah cocoon was degummed according to the method described in the literature [10,13,32]. It was then washed and dried with deionized water to obtain regenerated fibroin fibrin. This fibrin was dissolved in the ionic liquid [AMIM]Cl system and heated in an oil bath at 125 °C to form a 4.00 wt% tussah silk fibroin solution. Subsequently, the solution was treated with ultrasonic equipment at 600 W power. The device, equipped with a probe ultrasonic source featuring a 2 mm diameter titanium micro-tip, was positioned with the probe end 20 mm below the surface of the solution. Continuous ultrasound was applied for durations of 0, 15, 30, 45, and 60 min, respectively.

To control the solution temperature during ultrasonic treatment, the following regulation methods were used: 1) using a circulating ice water bath to maintain the stability of the solution temperature (<40 °C), 2) choosing optimized ultrasonic power for fabrication, such as 600 W, to reduce the generation of heat. In addition, a temperature sensor was used to monitor the solution temperature in real time to ensure effective control of the solution temperature during the sonication process. The evenly dispersed tussah silk spinning solution was then fed into the spray spinning device and processed at ambient temperature. The experiment parameters were follow: spinning head diameter at 1.5 mm, pressure at 0.9 MPa, flow rate at 15 mL/h, and receiving distance at 50 cm. The resultant tussah silk fiber film was immediately immersed in a flowing ice water bath, removed after 12 h, and rinsed three times with deionized water to eliminate any residual ionic liquid on the surface of the sample. It was then dried in an oven at 50 °C for 10 h to remove excess water. The final tussah silk fiber film samples were named C-0, C-15, C-30, C-45, and C-60, corresponding to the ultrasonic treatment times.

The power intensity of ultrasound varies with the ultrasonic power, and the actual output power (P_{US}) of the ultrasound will be less than its rated output power due to transmission losses in the medium during propagation. Therefore, the actual power intensity (I_A) of ultrasound can be calculated by the following Equations (1) and (2) [33]:

$$P_{US} = mC_p\frac{\Delta T}{t} \quad (1)$$

Table 1
Some research examples of biomaterials and innovative methods for promoting SDGs.

The Study Focus	Key Points	Targets of SDGs	Country	Reference
The effects of structures of silk, cellulose and chitin on green energy devices were studied.	Improvement of polymer structure and properties by chemical modification, such as the methanol-treated filipin generating 8 V in the open circuit with 5 μW/cm^2 power density.	SDG-7.2: By 2030, increase the share of renewable energy in the global energy mix substantially. SDG-12.2: By 2030, achieve the sustainable management and efficient use of natural resources.	China	[5]
The structure and properties of Bombyx mori mixed with Muga, Thai, Tussah and Eri silk were studied, respectively.	The content of α-helical structure in the film increased with the amount of other silks in the blends, which promoted the film's mechanical performance.	SDG-7.a: By 2030, strengthen international cooperation, promote clean energy research, technology and investment, and promote clean energy infrastructure investment.	United States	[10]
The effects of urea and sodium carbonate degumming methods on the structure and property of fibroin were studied.	The peak thermal decomposition, tensile strength and elongation of silk prepared using urea degumming method was raised to 296.50 °C, 276.66 cN and 2.93 %, respectively.	SDG-7.3: By 2030, double the global rate of improvement in energy efficiency	China	[13]
The potential of Bombyx silk nanofiber films and tussah silk fibers in guiding bone regeneration was studied by high-speed shearing method.	Tussah fibers with a diameter of 146.09 ± 63.56 nm exhibited high modulus and strength of 3.61 GPa and 74.27 MPa, individually, promoted bone cell adhesion and proliferation.	SDG-3.9: By 2030, substantially reduce the number of deaths and illnesses from hazardous chemicals and air, water and soil pollution and contamination.	China	[17]
The dissolution process influence on the structural and mechanical property of filamentous materials was investigated by comparing different methods of dissolution and processing of silk.	Ionic liquids are capable of disrupting hydrogen bonds between *β*-sheets structure, simplifying the regeneration process of SF, developing silk protein materials with tunable properties.	SDG-7.3: By 2030, double the global rate of improvement in energy efficiency.	China	[18]
The molecular structure and synthesis of imidazole and pyridine cations have been investigated to compare the polarity and hydrogen bonding capacity of ionic liquids associated with sugar solubilization and functionalization.	The ionic liquid has flexible conformation, economic and green preparation process, It can effectively dissolve biopolymers, spin them into fibers, and extrude them into plates.	SDG-7.a: By 2030, strengthen international cooperation, promote clean energy research, technology and investment, and promote clean energy infrastructure investment. SDG-12.4: Manage chemicals and wastes sustainably throughout their life cycle in accordance with global standards to significantly reduce emissions and minimize their harmful effects on health and the environment.	Brazilian	[23]
Ultrasonic-assisted drying was applied in the food processing to study the different ultrasonic experiment parameters on the physical and functional characteristics of protein.	Ultrasound-assisted drying reduces drying time, removes the mechanical stresses, low protein denaturation, and promotes a uniform particle size distribution resulting in a better gel network, raises the mass of small molecule proteins and decreases the charge density of protein.	SDG-2.1: By 2030, end hunger and ensure access by all people, to safe, nutritious and sufficient food all year round. SDG-7.3: By 2030, double the global rate of improvement in energy efficiency.	Iranian	[25]
The ultrasound time, frequency and intensity influence on the gelation, structure, emulsification and rheological properties of biopolymers was investigated.	Ultrasound can improve the emulsification properties, rheology, solubility, thermal stability, and bioactivity of biopolymer solutions.	SDG-7.3: By 2030, double the global rate of improvement in energy efficiency.	China	[26]
The ultrasonication time on the secondary structure and tensile property of silk fibers were investigated.	Ultrasonication promoted the carbonyl and oxygen content of the silk protein increasing, leading the *β*-sheets structure up to 40.93 %, which enhanced the loading force of the silk fibers to 245.9 N.	SDG-7.1: By 2030, ensure universal access to affordable, reliable and modern energy services. SDG-12.4: Manage chemicals and wastes sustainably throughout their life cycle in accordance with global standards to significantly reduce emissions and minimize their harmful effects on health and the environment.	China	[27]
The performance of chitin prepared as a wound healing accelerator by alkaline and ultrasonic treatments to control the degree of deacetylation and molecular weight of chitin was investigated.	The Mw of the ultrasonically treated chitin was 79.50 × 10^4, which was stable in aqueous solution and exhibited good biocompatibility, high tensile strength and efficient wound healing properties.	SDG-3.9: By 2030, substantially reduce the number of deaths and illnesses from hazardous chemicals and air, water and soil pollution and contamination. SDG-12.4: Manage chemicals and wastes sustainably throughout their life cycle in accordance with global standards to significantly reduce emissions and minimize their harmful effects on health and the environment.	South Korea	[28]
The morphology and properties of keratin composite films prepared by enzyme-ultrasound treatment were studied.	Smooth translucent composite films obtained under enzyme-ultrasound-assisted conditions showed good mechanical properties, and the elastic modulus of the films reached 35 MPa when the ratio of keratin to cellulose acetate was 5:95.	SDG-7.a: By 2030, strengthen international cooperation, promote clean energy research, technology and investment, and promote clean energy infrastructure investment. SDG-12.5: By 2030, substantially reduce waste generation through prevention, reduction, recycling and reuse.	Italy	[29]
The different ultrasound durations influence on the morphology, structure and properties of fibroin-soy protein composite nanofibers were investigated.	With the increase of ultrasound time, the fiber diameter decreased to 89 nm, the shift from random curl to *β*-sheets, up to 50.23 % content, and the mechanical property, thermal stability,	SDG-7.1: By 2030, ensure universal access to affordable, reliable and modern energy services. SDG-12.2: By 2030, achieve the sustainable	China	[30]

(*continued on next page*)

Table 1 (*continued*)

The Study Focus	Key Points	Targets of SDGs	Country	Reference
	hydrophilicity, and the biocompatibility of composite fibers were improved.	management and efficient use of natural resources.		
The ultrasonic-assisted dyeing parameters, such as power, temperature and immersion time influence on the crystallinity, thermal stability, and dye uptake of wood were investigated.	The best dyeing effect on wood was achieved under 50 °C, the ultrasonic power was 160 W, the dye concentration was 0.5 %, and the dyeing time was 120 min. The degree of crystallinity of the wood was increased to 50.52 %, and the thermal stability was improved.	SDG-7.1: By 2030, ensure universal access to affordable, reliable and modern energy services. SDG-12.4: Manage chemicals and wastes sustainably throughout their life cycle in accordance with global standards to significantly reduce emissions and minimize their harmful effects on health and the environment.	China	[31]

$$I_A = \frac{P_{us}}{A} \tag{2}$$

where m is the mass of the solution (kg), C_p is the specific heat capacity of the solution ($J{\cdot}kg^{-1}{\cdot}K^{-1}$), ΔT is the change in temperature of the solution before and after ultrasonication (°C), t is the time of ultrasonication (s), and A is the area of the ultrasonic wave propagation in the solution (m^2). It can be observed that the intensity of ultrasound is related to the ultrasonic treatment time t and frequency f at constant rated ultrasound power. Under the action of ultrasound, the tiny bubble nuclei in the solution undergo the sparse phase and compressed phase of ultrasound, grow and shrink in volume, and accumulate. When the acoustic pressure exceeds the threshold, the bubbles collapse, generating transient high temperatures and pressures. This can accelerate the rate of mass transfer between interfaces and the efficiency of non-homogeneous phase reactions [26]. The kinetic energy of the cavitation bubbles can be calculated from Equation (3) [34,35]:

$$K = \frac{1}{2}\rho\int_{R}^{\infty} u^2 A\hat{A}{\cdot}4\pi r^2 dr = 2\pi\rho U^2 R^3 \tag{3}$$

where ρ is the density of the medium, R is the radius of the bubble, u is the velocity at any distance r (greater than R) from the center of the bubble, and U is the surface velocity at time t. In addition, the size of the cavitation bubble is related to the acoustic pressure, hydrostatic pressure, frequency and the density of the liquid as shown in the following Equations (4) and (5) [35]:

$$R_r = \left(\frac{3\gamma P_\infty}{\rho\omega^2}\right)^{\frac{1}{2}} \tag{4}$$

$$R_{max} = \frac{4}{3\omega_a}(P_a - P_h)\left(\frac{2}{\rho P_a}\right)^{\frac{1}{2}}\left[1 + \frac{2}{3P_h}(P_a - P_h)\right]^{\frac{1}{3}} \tag{5}$$

where R_r and R_{max} are the minimum and maximum dimensions of the bubble at the time of collapse, respectively. γ is the specific heat ratio of the gas inside the bubble, ω is the angular frequency of the ultrasonic wave, and P_a is the acoustic pressure amplitude. P_∞ and P_h are the ambient liquid pressure and hydrostatic pressure, respectively. Furthermore, it is assumed that the bubble expands isothermally and that the vapor pressure inside the bubble remains constant, with no transfer of mass or heat during the rupture process [36]. Based on this assumption, an approximation of the maximum internal temperature (T_{max}) and pressure (P_{max}) at the end of the bubble collapse can be calculated using the adiabatic law, dependent on the bubble's size, as shown in Equations (6) and (7) [36]:

$$T_{max} = T_\infty\left(\frac{R_{max}}{R_r}\right)^{3(\gamma-1)} \tag{6}$$

$$P_{max} = \left[P_v + P_{g0}\left(\frac{R_0}{R_{max}}\right)^3\right]\left(\frac{R_{max}}{R_r}\right)^{3\gamma} \tag{7}$$

where T_∞ is the temperature of the liquid, P_v is the saturated vapor pressure, R_0 is the radius of the bubbles in the solution, and P_{g0} is the gas pressure inside the bubbles in the solution ($R{=}R_0$).

Through the density of the medium (ρ) and ultrasonic frequency (ω), the bubble radius at any distance (r) from the center of the bubble can be obtained (Equations (4) and (5)). Then, according to Equations (6) and (7), the pressure and temperature at which the bubbles collapse during ultrasonication can be predicted. It was shown that the larger the radius of the bubble at the time of collapse, the higher the internal temperature and pressure of the SF solution. Therefore, by adjusting the ultrasonic conditions (e.g., ultrasonic power, treatment time), the bubble behavior can be controlled, affecting the microstructure and macroscopic properties of the material.

2.3. Materials characterization

2.3.1. Scanning electron microscopy

Scanning electron microscopy (SEM, JSM-7600F, JEOL, Japan) was utilized to observe the morphology of the tussah silk fiber membranes treated with various durations of ultrasound. Initially, the samples were affixed on the sample stage using conductive carbon double-sided tape and then coated with gold in a sputter coater (JFC-1600, JEOL, Japan) at a current of 20 mA, with each side plated four times for 20 s. The coated samples were transferred to the SEM chamber and observed under high vacuum at room temperature, with the SEM operated at voltages between 5 and 10 kV. SEM images of samples were processed with Image J software, and each sample's fiber diameter and surface area were calculated from at least 100 measurements to accurately determine the average values. The average fiber diameter (D) and average surface area (A) was calculated using Equations (8) and (9), respectively, as follows:

$$D = \frac{\sum_{i=1}^{i} d_i}{i} \tag{8}$$

where i is the number of fibers with diameter d_i.

$$A = \frac{\sum_{i=1}^{i} A_i}{n} \tag{9}$$

where i is the number of fibres with diameter d_i, and n is the analysis times of the sample.

2.3.2. Fourier transform infrared spectroscopy

A Fourier Transform Infrared Spectrometer (NEXUS-670, Nicolet, USA) equipped with a multi-reflectance stage ATR accessory (OMNIT, Ge crystal) was employed to acquire infrared spectra of the tussah silk fiber membrane samples. Background spectra were collected prior to each session, with a resolution of 4 cm^{-1} from 4000 cm^{-1} to 400 cm^{-1}, scanning each sample 64 times. The resulting spectra were baseline-corrected and atmosphere-compensated using Origin software, with the quantification of secondary structures performed by Gaussian fitting of the amide I region. Fittings were repeated at least five times to achieve a Chi^2 factor less than 10^{-4}.

2.3.3. X-ray diffraction analysis

X-ray diffraction measurements were performed using an XRD diffractometer (D/max 2500/PC, Rigaku, Japan) at room temperature. The device employed Cu Kα radiation at a tube pressure of 40 kV and a current of 150 mA, scanning from 5° to 60° (2θ) at a speed of 10°/min.

2.3.4. Differential scanning calorimetry

The thermal properties of the ultrasound-spun tussah silk fiber membrane samples were measured using a simultaneous thermal analyzer (STA7300 TG-DTA, Hitachi, Japan). Each sample, weighing approximately 3 mg, was sealed in a crucible. Under standard DSC conditions, the samples were heated from room temperature to 550 °C in a nitrogen atmosphere (flow rate of 30 mL/min) at a heating rate of 10 °C/min. The glass transition processes were analyzed using temperature-modulated differential scanning calorimetry (TM-DSC) with a differential scanning calorimeter (DSC700X+RV model, Hitachi, Japan). The TM-DSC conditions were as follows: a nitrogen flow rate of 50 mL/min, and heating from −20 °C to 250 °C at a rate of 5 °C/min, with a frequency and temperature amplitude of 0.02 Hz and 3 °C, respectively. The specific heat capacity was calibrated using aluminum and sapphire standards. All crucibles were maintained at the same weight (±0.1 mg difference).

2.3.5. Thermogravimetric analysis

Thermogravimetric analysis was performed using a Pyris 1 analyzer (PerkinElmer, USA) to measure the mass change in tussah silk fiber membrane samples as temperature increased. Calibration was performed using aluminum, nickel, and calorimetry standards, with three repetitions to ensure temperature accuracy within ± 0.5 °C. Conditions for the thermogravimetric (TG) curve included a nitrogen flow of 50 mL/min, a heating rate of 10 °C/min, a temperature range from room temperature to 550 °C, and a sample mass of about 3 mg. The curve documented the percentage change in sample mass during heating. Additionally, a first-order derivative curve (DTG) was derived to reflect the thermal decomposition rate of the samples.

2.3.6. Nanoindentation analysis

Nanoindentation tests were conducted on tussah silk fiber membranes using an atomic force microscope (AFM5000 II, Hitachi, Japan) to evaluate their mechanical properties at the microscopic scale. Initially, samples were cast onto a mica sheet, and a 10 × 10 μm^2 area of the sample surface was scanned in tapping mode. Indentation was performed using a 10 nm radius orb tip. Given that the mechanical properties derived from nanoindentation are sensitive to tip geometry, a standard polycarbonate sample was used to calibrate the tip area function following standard methods before assessing the sample's properties. The loading and unloading rate used during indentation was 2000 nN/s, with a constant hold time at peak load of 0.5 s, and peak loads ranged from 2800 nN to 5200 nN. At least five indentations were made on different areas of each sample's surface to ensure accuracy. The hardness (H) and elastic modulus (E_s) were calculated based on the average data obtained from these measurements using the following equations (10–12).

The hardness (H) of the sample can be calculated from Equation (10) [37,38]:

$$H = \frac{P_{max}}{A} \tag{10}$$

where $P_{\max}$ is the maximum load and A is the tip area as a function of the tip area of the fused silica sample calibrated according to standard procedures. The reduced modulus (E_r) and elastic modulus (E_s) of the samples are closely related to each other from Equations (11) and (12) [39–41]:

$$\frac{dP}{dh} = \frac{2Er \times \sqrt{A}}{\sqrt{\pi}} \tag{11}$$

$$E_s = \frac{1 - V_S^2}{\frac{1}{E_r} - \frac{1-V_i}{E_i}} \tag{12}$$

where E_r is determined by best fitting the plotted curve and dP/dh is the slope of the best fit to the force unloading curve. E is the elastic modulus, v is Poisson's ratio, and the subscripts i and s denote the indenter and sample, respectively. The Poisson's ratio of the sample $v_s = 0.38$. For the round ball tip used in this study $v_i = 0.07$, $E_i = 1140$ GPa [40,42]. In addition, we obtained the recovery force of tussah silk fiber samples by calculating the ratio of the area under the unloading curve (A_1) and the area under the compression curve (A_2) in the force distance curve [43], as shown in Equation (13):

$$Resilience = \frac{A_1}{A_2} \times 100\% \tag{13}$$

2.3.7. Water contact angle

The water contact angle was tested on the surface of the tussah silk fiber membrane using a water contact angle meter (WCA, DSA30S, Kruss, Germany). The procedure involved dropping 2 μL of pure water onto the surface of each sample to determine their surface wetting characteristics after various durations of ultrasonic treatment. The water contact angle for each sample was measured at least three times to ensure accuracy in calculating the average value.

2.3.8. Cytotoxicity and biocompatibility

L929 (mouse fibroblast) cells were used to assess the biocompatibility of tussah silk fiber membrane samples. Initially, the membranes were cut into appropriate sizes and sterilized on an ultra-clean bench alongside a 96-well plate for 1 h. Subsequently, the samples were immersed in a 75 % ethanol solution and exposed to UV light irradiation for 1 h. After irradiation, the treated membranes were placed at the bottom of a 96-well plate. The ethanol was then removed, and the plate was rinsed three times with PBS solution. The cultured L929 cells were detached using trypsin, suspended at a concentration of 1 × 10^4 cells/cm^3 in fresh culture medium containing 10 % vol fetal bovine serum and 1 % vol double antibody, and 200 μL of this cell suspension was inoculated onto each tussah silk fiber membrane. The samples were then incubated in a cell culture incubator at 37 °C and 5 % CO_2 for 6, 24, and 48 h. Subsequently, 200 μL of 0.5 mg/mL thiazolyl blue (MTT) solution replaced the incubation solution and was incubated for 4 h. Afterwards, the MTT solution was discarded, and 200 μL of dimethyl sulfoxide (DMSO) was added to dissolve the formazan crystals by shaking at room temperature for 10 min. The absorbance at 570 nm for each well was measured using an enzyme-linked immunoassay analyzer (EL-X800, BioTek, USA). Three sets of parallel samples were tested for each membrane, and the average absorbance was calculated and compared with a control group that contained no sample. Cell viability was determined using Equation (14) [44]:

$$Viability(\%) = \frac{D_s}{D_c} \times 100\% \tag{14}$$

where D_s is the absorbance of the sample group and D_c is the absorbance of the control group.

2.3.9. Biodegradability

Protease E was dissolved in PBS buffer (pH 7.4) to prepare a protease solution with a concentration of 0.2 mg/mL. The tussah silk fiber membrane samples were then placed into centrifuge tubes containing 5 mL of deionized water, PBS buffer, and protease solution, respectively, and were incubated in a 37 °C constant temperature water bath. After 1, 2, 3, and 5 days, the samples were removed from the environment, thoroughly rinsed with distilled water, and dried in a vacuum desiccator until a constant weight was achieved. The samples were then weighed to estimate the degree of degradation. Throughout the degradation

process, the protease solution was periodically refreshed to ensure optimal enzyme activity. The percentage of degradation was calculated using the following Equation (15):

$$Degradation(\%) = \left(\frac{M_i - M_r}{M_i}\right) \times 100\% \quad (15)$$

where M_i is the initial mass of the sample and M_r is the remaining mass of the sample after degradation.

2.3.10. Solution viscosity test

The viscosity of TSF solutions after ultrasonic treatment for 0, 15, 30, 45, and 60 min was measured using a rotary viscometer (NDJ-9S, Shanghai Fang Rui Instrument Co., Ltd., China). To conduct the test, 10 ml of each solution was poured into the sample cell, with the solution temperature maintained at 40 °C and the rotor speed set at 30 rpm. Each measurement was performed at least three times to ensure accuracy.

3. Results and discussion

3.1. Surface morphology

The morphology of tussah silk fiber membranes after ultrasonic spray spinning based on AMIMCl ionic liquid system was observed by SEM at different time durations. As shown in Fig. 2a, for the untreated tussah silk fibrous membrane (C-0), the surface was uneven, rough, and grooved; the fiber morphology was not uniformly distributed, and the fibers were interlaced and collapsed together. This is primarily due to a more intertwined molecular chains structure for tussah silk, which leads to increased solution viscosity and challenges in jet splitting [45], making tussah silk difficult to stretch and form during jet spinning. In contrast, for the ultrasonically treated samples (C-15), the adhesion and collapse between fibers began to diminish (Fig. 2b), with the fiber diameter decreasing from 1.87 ± 0.17 μm (C-0) to 1.49 ± 0.11 μm (C-15), and the fiber surface area increasing from 36.60 ± 3.89 μm^2 (C-0) to 53.56 ± 3.31 μm^2 (C-15) as shown in Fig. 2 and **Fig. S1**. The fiber diameter of the untreated C-0 sample is mainly between 1.78 and 2.00 μm (83.02 %), while the C-60 sample, treated with ultrasound at 600 power for 60 min, is mainly between 0.85 and 0.95 μm (79.7 %). This improvement may be attributed to ultrasonic treatment promoting the dissolution of tussah proteins and reducing the viscosity of the solution (**Fig. S2**), which positively impacts the formation of fibers by jet stretching in the spray-spun solution. The results from the viscosity experiment showed that the viscosity decreased from approximately 0.4 Pa·s for the untreated sample to about 0.2 Pa·s after 60 min of ultrasonic treatment (**Fig. S2**). For instance, He *et al.* [46] observed that the molecular structure of tussah silk and the entanglement of molecules significantly affected the stretching and shaping of fibers, leading to bifurcation, adherence, and collapse of the composite fibers. Similarly, Iida *et al.* [47] found that ultrasonication reduced the viscosity of a starch solution by approximately two orders of magnitude to 100 mPa·s. Wang *et al.* [48], while preparing alginate/chitosan fiber scaffolds, noted that the diameter of the fibers decreased with the solution's decreasing viscosity. Furthermore, as the ultrasonication time increased from 15 min to 60 min, the adhesion and collapse of the fibers gradually decreased, and the fibers became flatter and smoother (Fig. 2b ~ **2e**). For example, the sample C-60 exhibited uniform fiber morphology and a smooth fiber surface (Fig. 2e). The average fiber diameter and surface area of tussah silk samples also changed with the increase in ultrasound time (Fig. 2**f, g**): the fiber diameter decreased from 1.49 ± 0.11 μm (C-15) to 0.90 ± 0.07 μm (C-60), while the fiber surface area increased from 53.56 ± 3.31 μm^2 (C-15) to 67.04 ± 3.09 μm^2 (C-60).

These changes indicate that ultrasonic treatment can significantly affect the surface morphology, size (Fig. 2) and diameter distribution (**Fig. S1**) of fibers. The likely reason for these effects is that prolonged ultrasonic treatment weakens the entanglement between molecular chains, reducing the solution's viscosity and enhancing dissolution. This promotes uniform dispersion and rearrangement of molecular chains in the regenerated silk fibroin solution. Particularly during solution spinning or film-making processes, more ordered β-sheets and α-helical structures are formed, potentially smoothing and regularizing the surface and structure of the tussah silk material [49,50]. Additionally, several studies [30,51] have demonstrated that fibers with a higher surface area are more conducive to cell adhesion, and growth, as well as multiplication, making them highly suitable for biomedical applications.

3.2. Structural analysis

FTIR and XRD are commonly used as effective tools in protein polymer structure analysis [29,48]. FTIR was first utilized to analyze the

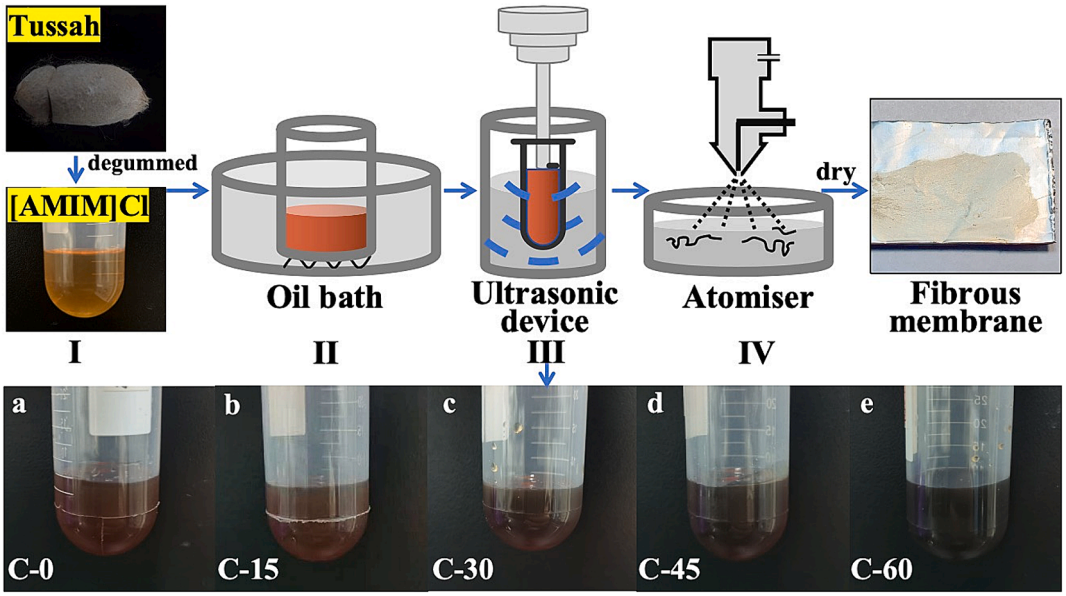

Fig. 1. Flow chart of the ultrasonic spray spinning fabrication of tussah silk fiber membranes based on an ionic liquid system (Stages I-IV). Regenerated tussah silk solutions after long-term ultrasound treatment at various durations (0 min (a), 15 min (b), 30 min (c), 45 min (d), 60 min (e)).

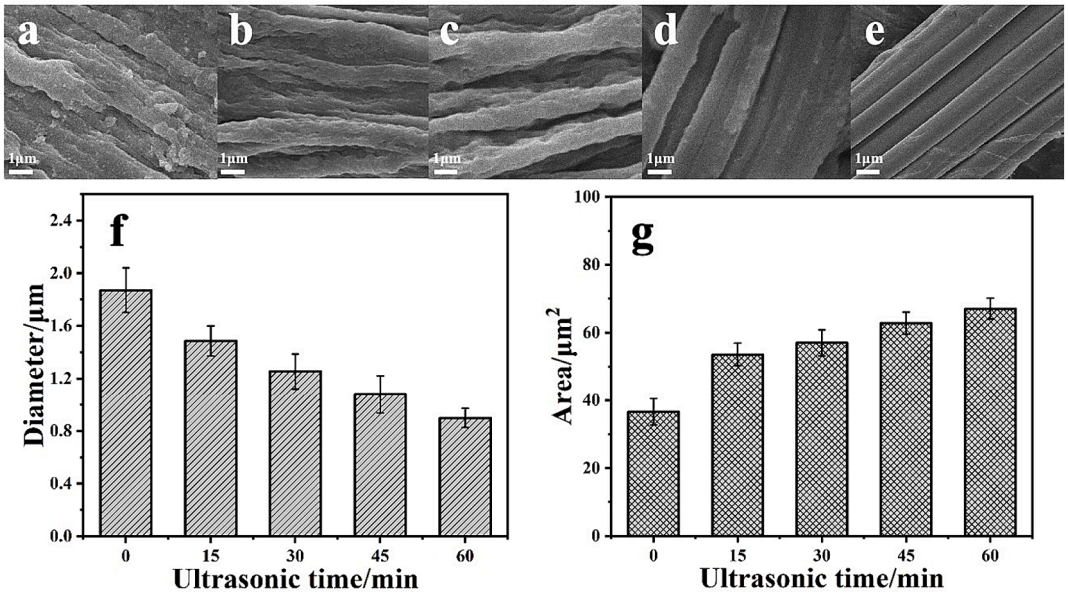

Fig. 2. SEM images of TSF samples after ultrasonic treatment for different durations: C-0 (a), C-15 (b), C-30 (c), C-45 (d), and C-60 (e), with a scale of 1 μm, and their average fiber diameter (f) and fiber surface area (g).

effects of varying ultrasound treatment durations on the secondary structure of tussah silk fiber membranes. Typically, there are three main amide regions in the infrared spectrum of silk proteins: the Amide I band (1710–1590 cm^{-1}), mainly influenced by C=O and C-N group stretching vibrations; the Amide II band (1590–1500 cm^{-1}), characterized by C-C and C-N stretching and N-H bending vibrations; and the Amide III band (1350–1200 cm^{-1}), which varies depending on the side-chains and hydrogen bonding, primarily involving C-C-N bending [52,53]. As illustrated in Fig. 3a, the absorption peak values of the tussah silk fiber membrane samples shifted with increasing ultrasonic time, with the peak in the Amide I band moving from 1626 cm^{-1} in sample C-0 to 1620 cm^{-1} in sample C-60, and the peak in the Amide II band shifting from

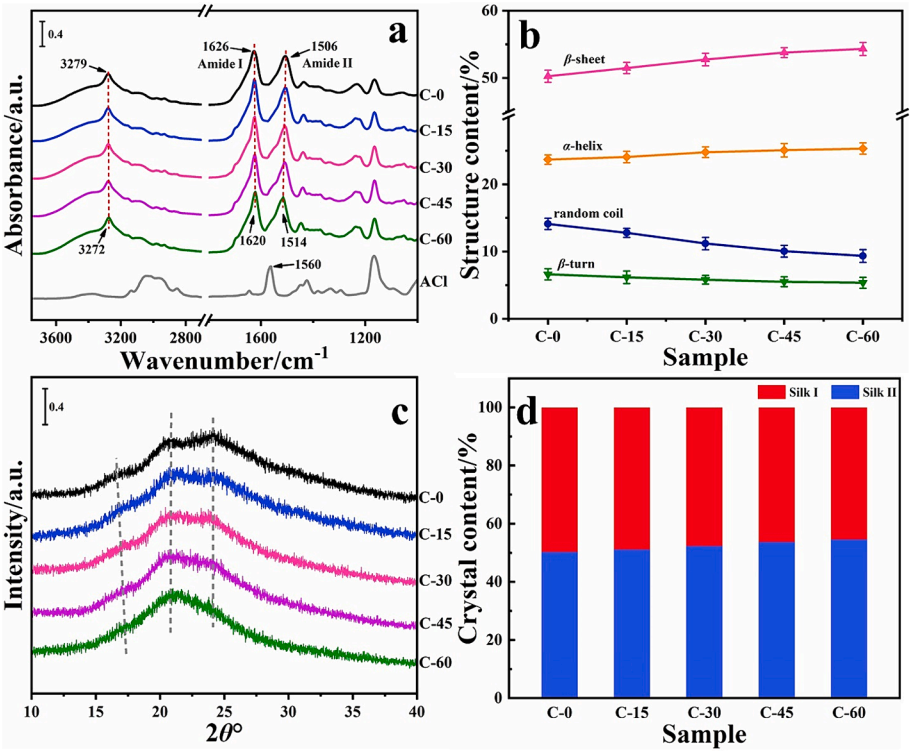

Fig. 3. FTIR spectra of tussah silk fibrous membranes treated with different durations of ultrasound (0–60 min) in the wavelength range of 3800–1000 cm^{-1} (a), and the content of secondary structures in tussah silk fibrous proteins calculated by curve fitting in the Amide I region (b), with pink upper triangles, orange diamonds, blue circles, and green lower triangles representing β-sheets, α-helix, random coils, and β-turns, respectively. The XRD spectra of the fibrous membrane samples in the range of $2\theta = 10°$-$50°$ (c), and the contents of Silk I and Silk II in tussah silk fibrous membranes calculated from the XRD curves (d), where the red and blue colors represent the crystal forms of Silk I and Silk II, respectively. (For interpretation of the references to colour in this figure legend, the reader is referred to the web version of this article.)

1506 cm^{-1} (C-0) to 1514 cm^{-1} (C-60). Additionally, peak intensities within the Amide I and II bands became sharper with extended ultrasonic time. This suggests that ultrasonication modifies the structure of tussah silk proteins, and the shifts in absorption peaks within the Amide I band may be caused by changes in the structural content of α-helices, β-sheets, and random coils [14,54].

IR spectral fitting quantified the secondary structure contents in proteins. The Amide I band, being the most intense absorption band, typically reflects the silk protein conformation as follows: β-sheets at 1637–1616 cm^{-1} and 1703–1697 cm^{-1}, random coils at 1655–1638 cm^{-1}, α-helices at 1662–1656 cm^{-1}, β-turns at 1696–1663 cm^{-1}, and side chains at 1615–1605 cm^{-1} [53,55]. To further understand the impact of ultrasonic time on the secondary structure of tussah silk proteins, peaks were fitted to the spectra in the amide I band (1590–1710 cm^{-1}) (Fig. S3a). The variation in the secondary structure content of the tussah silk fiber membrane samples is depicted in Fig. 3b and **Table S1**, with the total β-sheet content being notably high (>50 %) across all samples. With increased ultrasonic time, the total β-sheet content rose from 50.26 % in sample C-0 to 54.32 % in C-60, while the content of α-helices also increased, and that of random coils decreased from 14.11 % in C-0 to 9.36 % in C-60. This shift was attributed to localized high heat and energy during ultrasonication, which promoted the transformation of molecular conformations from Silk I to the more stable Silk II type, enhancing the β-sheet and α-helix contents in the amide I bands and reducing the disordered structures.

Prolonged ultrasound exposure also enhanced hydrogen bonding interactions among molecular chains of tussah silk proteins [27,56,57]. Different solvents can also impact the secondary structure content in tussah silk fiber membrane samples [58]. For instance, after the sample was removed from the ice bath, it was washed with a methanol solution instead of deionized water to remove residual ionic liquids. The FTIR spectrum and calculated secondary structure content were presented in **Fig. S4**, respectively. It was observed that the peak intensity in the Amide I band of methanol-treated samples was lower than that of water-treated samples, and the peak in the Amide II band shifted to near 1560 cm^{-1}. IR fitting revealed that methanol-treated samples had higher β-turns and lower total β-sheets compared to water-treated samples (Fig. S4c). This difference is attributed to methanol's lower polarity compared to water, which hinders the silk fibroin chains' ability to form β-sheet structures during treatment. Goujon *et al.* [58] corroborated this finding, noting that water promotes the formation of more β-sheet structures in regenerated tussah silk membranes compared to methanol, resulting in a more stable Silk II structure. To further explore the influence of ultrasonic treatment on the structure and properties of silk fibroin, we selected samples treated for different durations and washed with deionized water to continue this study.

The crystal structure of tussah silk fiber membranes was further explored via XRD. In the polymerized state, SF is a macromolecular chain consisting of partially repeated sequences of crystalline and amorphous regions [18]. The absence of a regular crystal structure in the SF molecular chain leads to low-intensity diffraction peaks and the presence of broad peaks corresponding to disordered regions [56,59]. The XRD patterns of the tussah silk fiber membranes after varying durations of ultrasonication are shown in Fig. 3c. Studies have indicated that silk possesses two crystalline forms, Silk I and Silk II, with the main conformation of Silk II being an antiparallel β-sheet structure, corresponding to diffraction angles 2θ around 16.8°, 20.4°, 23.8°, and 30.9°. Conversely, Silk I is generally considered a combination of random coils, α-helices, and β-turns with major diffraction peaks around 11.9°, 22.0°, 24.7°, and 27.9° [60,61].

From Fig. 3c, it is evident that all tussah silk fiber membrane samples exhibited similar XRD spectra. For the untreated samples (C-0), diffraction peaks appeared near 16.7° (Silk II), 20.8° (Silk II), and 24.1° (Silk I). With increasing ultrasonic time, the peak at 16.7° gradually shifted to 17.2° and the intensity of the 20.8° peak increased, indicating an enhancement of the Silk II structure. Additionally, the intensity of the Silk I diffraction peak near 24.1° significantly decreased. The diffraction angles corresponding to Silk I and Silk II structures were selected for peak fitting (Fig. S3b), and the results from the fitting calculations (Fig. 3d, **Table S2**) paralleled those from the FTIR fitting (Fig. 3b, **Table S1**).

The XRD results confirmed that ultrasonication affects the crystal structure of the samples, with a decrease in Silk I content, and a raising in Silk II structure (β-sheets) as ultrasonic time increased from 0 to 60 min. Moreover, Wang *et al.* [62] found that high ultrasonic power promotes a conformational shift in silk fiber proteins, further supporting that ultrasonication enhances hydrogen bonding interactions in the membrane of tussah silk fibers and promotes the transition from the randomly coiled structure to the stable β-sheets and sub-stable α-helices.

3.3. Thermal property analyses

The samples were analyzed using DSC and TM-DSC to determine the thermal properties of the tussah silk fiber membranes after various durations of ultrasonic treatment, with the results displayed in Fig. 4. The standard DSC curve (Fig. 4a) revealed two heat absorption peaks for all membrane samples: one between 30 °C and 150 °C, attributed to the evaporation of most bound water during the heating process [60], and another between 230 °C and 300 °C, associated with the onset of thermal degradation. The peak temperature of heat absorption (T_p) shifted towards higher temperatures in all ultrasonically treated samples compared to those without ultrasound treatment (Fig. 4a).

Fig. 4b displays the reversible heat capacity curves of tussah silk fiber membranes prepared at different ultrasound durations. The glass transition temperature (T_g) is determined by the midpoint of the reversible heat capacity step, and the increase in this region indicates the heat capacity increment (ΔC_p) [63]. Further analysis showed that T_g decreased from 207.38 °C in sample C-0 to 202.42 °C in sample C-60 with increasing sonication time, and ΔC_p also decreased from 0.1096 J/g·°C to 0.0443 J/g·°C (Table 2). The polymer chains will exhibit new thermal transitions depending on the structure formed after ultrasound treatment in the IL solution. This decrease in T_g suggests that prolonged ultrasound maybe reduce the internal entanglement between different molecular chain regions, allowing the local movement of these chain regions more easily and causing the glass transition to occur at lower temperatures [64]. Moreover, the energy generated by the ultrasound enhances the vibration of polymer amorphous molecular chains in the regenerated SF more easily at the microscopic level, thus enhancing the mobility of molecular chains as the material is heated, and lowering the temperature required for reaching the glass transition state [65]. Conversely, the reduction in ΔC_p indicates a decrease in the random coil structure within the tussah silk fiber membranes, consistent with FTIR analysis results. Other studies [27,56,62] have also confirmed that ultrasonication duration influences structural changes in tussah silk fiber materials.

Bio-nanofibers are widely used in biomedical and tissue engineering fields, especially in the manufacture of medical devices or implants that require high-temperature disinfection and sterilization, where the thermal stability of the material is an important performance indicator. For example, biomaterials with high thermal stability can maintain structural and functional integrity during high-temperature treatment, ensuring the safety and reliability of medical products. In order to further evaluate the thermal stability of tussah silk nanofiber membranes post-ultrasound treatment, all samples underwent thermogravimetric (TG) analysis.

Fig. 4c and 4d illustrate the mass percentage change curves and their DTG curves, respectively, for membranes heated from 30 °C to 550 °C under different ultrasound durations. Overall, the mass loss in the TG curves can be segmented into three zones: in Zone I (30 °C-200 °C), the sample weight decreases by approximately 3 % due to water evaporation. In Zone II (200–350 °C), the curves nearly linearize, and the weight loss decreases significantly with temperature, likely due to weakening

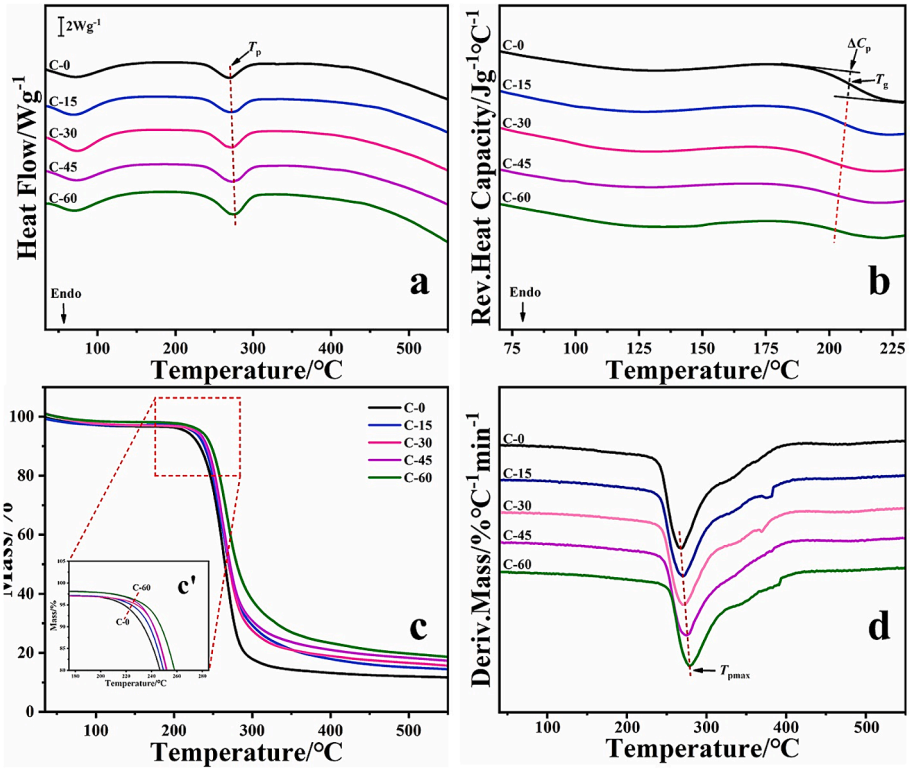

Fig. 4. DSC curves (a), TM-DSC curves (b), TG curves (c), and DTG curves (d) of tussah silk fiber membranes under various ultrasound treatments (0–60 min). T_p represents the peak endothermic temperature on the DSC curve, T_g and ΔC_p are the glass transition temperature and the heat capacity increment obtained from TM-DSC testing, respectively, and T_{pmax} represents the maximum weight loss temperature on the DTG curve.

Table 2
Thermodynamic parameters of tussah silk fiber membranes prepared by ultrasonic spray spinning.

Sample	T_{onset}/°C	T_{pmax}/°C	ΔY/%	m_{550}/%	T_p/°C	T_g/°C	ΔC_p/Jg^{-1}°C^{-1}
C-0	245.29	268.25	3.02	11.64	271.28	207.38	0.1096
C-15	249.32	269.67	2.97	14.41	272.17	206.29	0.0667
C-30	250.85	272.93	2.83	15.66	273.58	204.76	0.0559
C-45	252.63	276.41	2.05	17.43	274.76	203.69	0.0510
C-60	256.38	280.82	2.03	18.68	275.83	202.42	0.0443

intermolecular interactions and peptide bond cleavage [66]. Both the initial decomposition temperature (T_{onset}) and the maximum weight loss rate temperature (T_{pmax}) increased with longer ultrasound times; for example, the initial decomposition temperature rose from 245.29 °C in the untreated sample (C-0) to 256.38 °C in the sample treated for 60 min (C-60), and the maximum weight loss temperature increased from 268.25 °C to 280.82 °C (Fig. 4d, Table 2). In Zone III (350 °C-550 °C), the films continued to decompose, although the rate of weight loss was reduced. These results showed that long-term ultrasonic treatment promoted the formation of more ordered crystal structures, which effectively resisted decomposition at high temperatures and improved the thermal stability of the samples. This improvement was reflected not only in the increase of T_{onset} and T_{pmax} but also in the increase of residual mass of the sample at 550 °C.

Initial thermal decomposition temperature (T_{onset}), maximum weight loss temperature (T_{pmax}), moisture content (ΔY), and the remaining mass of the sample at 550 °C (m_{550}) are derived from the TGA curve. T_p represents the peak temperature of endothermic degradation observed in the DSC curve. T_g is the glass transition temperature value obtained through TM-DSC testing. ΔC_p denotes the specific heat capacity measured on the TM-DSC curve. Each sample were tested at least 3 times. All numbers are presented with an error margin of ± 2 %.

3.4. Mechanical property analysis

Hardness is defined as the ability of a material to resist localized deformation, specifically from a hard object being pressed into its surface. The elastic modulus is an important measure of an object's capacity to resist elastic deformation and reflects the strength of the bonds between atoms, ions, or molecules [67]. As ultrasonication time increases, the interactions and structural changes among tussah silk protein molecules can alter the material's mechanical properties. Fig. 5a displays the force-distance curves for samples C-0 and C-60, illustrating that the deflection of the cantilever tip depends on the surface position of the fibrous membrane. For each fiber membrane sample, at least five indentation tests were performed on different surface areas, calculating the hardness (H) and elastic modulus (E_s) for the samples, along with the standard deviation (Fig. 5).

The hardness and elastic modulus of the tussah silk fiber membrane samples are shown in Fig. 5b and Fig. 5c, respectively. For the non-ultrasonicated sample (C-0), the hardness and elastic modulus were 10.56 ± 0.61 GPa and 0.55 ± 0.035 GPa, respectively, with a reduced modulus of 0.64 ± 0.041 GPa (**Fig. S5**). As ultrasonic treatment time increased, the hardness of the samples rose from 11.21 ± 0.67 GPa for C-15 to 16.49 ± 0.41 GPa for C-60, and the elastic modulus increased from 0.58 ± 0.054 GPa (C-15) to 0.75 ± 0.037 GPa (C-60). Consequently, the

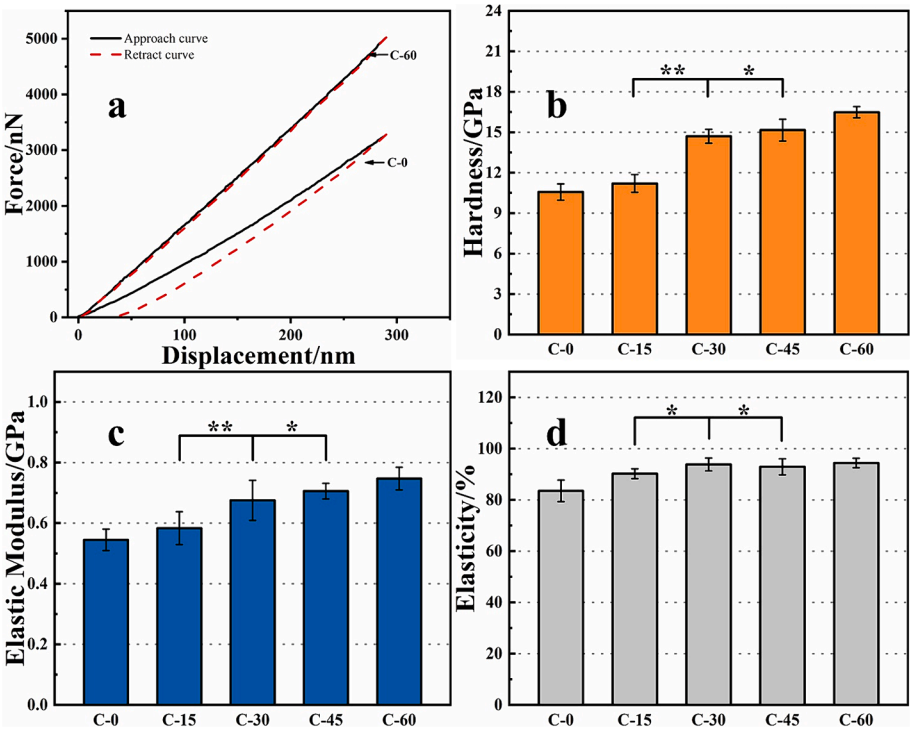

Fig. 5. Force-distance curves of tussah silk fiber membrane samples C-0 and C-60 (a), and the hardness (b), elastic modulus (c), and resilience (d) of the tussah silk fiber membrane samples at different ultrasound times (*p < 0.05, p < 0.01).

fiber membrane samples treated with 60 min of ultrasound exhibited the highest hardness and elastic modulus. The nanoindentation test results demonstrated that the mechanical strengths of the ultrasonically treated tussah silk fiber membranes were superior to those of the non-ultrasonicated samples, and these advantages amplified with longer ultrasonication times.

Resilience is defined as the energy recovered after removing the load, divided by the total deformation energy [43,68]. Fig. 5d shows the resilience of each sample. Compared to the resilience of sample C-0 without ultrasound (83.5 %), the resilience of sample C-15 increased by 6.7 %. With the ultrasound treatment time extended to 60 min, the resilience of sample C-60 reached its peak at 94.4 %, surpassing that of high-elasticity synthetic rubbers like polybutadiene (80 %) [68]. These results indicate that all samples exhibit high resilience, with those treated with ultrasound performing better in terms of resilience.

The enhancements in mechanical properties of the tussah silk fiber membrane samples were attributed to the transformation of the non-crystalline regions of the tussah silk protein chains into highly ordered β-sheet structures, facilitated by inter- and intramolecular interactions such as van der Waals forces, hydrogen bonding, and hydrophobic interactions under ultrasound [62,69,70]. Additionally, prolonged ultrasound treatment can further increase the protein chain orientation and crystallinity, resulting in a higher elastic modulus. This is supported by findings from researchers like Wang *et al.* [71], who observed that ultrasonic treatment not only increases the β-sheet content but also enhances the crystallinity of filamentous fibrous proteins. Similarly, Sakai *et al.* [72], in their study on the mechanical properties of gels, discovered that the high elastic modulus of the gels was due to the transformation of secondary structures within the gels to β-sheets.

3.5. Biological properties

The effects of ultrasonication time on the biological properties of tussah silk materials, specifically their hydrophilicity, cytocompatibility, and biodegradability, were thoroughly investigated. Surface wettability (hydrophilicity) is critical for biomaterials, affecting cell adhesion, proliferation, growth, and migration, and thereby significantly impacting their biomedical applications [73,74]. The surface wettability of the tussah silk fiber membrane samples was assessed by the water contact angle measurements (Fig. 6a). Tussah silk molecules contain many hydrophilic groups such as amino (–NH_2), hydroxyl (–OH), and carboxyl (–COOH) groups.

The untreated tussah silk sample (C-0) displayed a water contact angle of 82.6°, indicating moderate wettability. With increasing ultrasonication time, the water contact angle steadily decreased from 65.3° (C-15) to 43.8° (C-60), showcasing enhanced surface wettability. This increase in hydrophilicity may be attributed to ultrasound's mechanical and cavitation effects, which rearrange hydrophobic and hydrophilic regions within the protein molecules, thus improving the samples' wettability. Longer ultrasonication periods maybe intensified these effects, bringing more hydrophilic functional groups to the material's surface [57,74]. Moreover, SEM images (Fig. 1) also revealed that ultrasonically treated tussah silk fibers exhibited a high surface area for the fibers, which enhanced water absorption and penetration. In addition, roughness can also increase the water contact angle of the membrane material and enhance its hydrophobic properties. For example, in our study, a rough fiber mat demonstrated greater hydrophobicity (C-0), whereas a fiber mat with a flat and smooth surface showed better hydrophilicity (C-60).

In vitro cell proliferation assays are crucial for evaluating the cytocompatibility of biomaterials [69]. The biocompatibility and cell viability of tussah silk fiber membrane samples post-various ultrasonication periods were tested using L929 fibroblast cells. The cell viability on these samples (C-0, C-15, C-30, C-45, and C-60) over 6, 24, and 48 h is shown in Fig. 6b. Viability increased over time for all samples, particularly for those treated with ultrasound. For instance, the viability percentages for sample C-0 were 104.14 %, 111.31 %, and 117.29 % at 6, 24, and 48 h, respectively. In contrast, the ultrasound-treated C-60 samples exhibited significantly higher viability increments by 27.5 % (6 h), 28.43 % (24 h), and 35.79 % (48 h) compared to C-0. This trend suggests enhanced cell adhesion and proliferation on surfaces treated with longer ultrasound exposures. For example, after 45

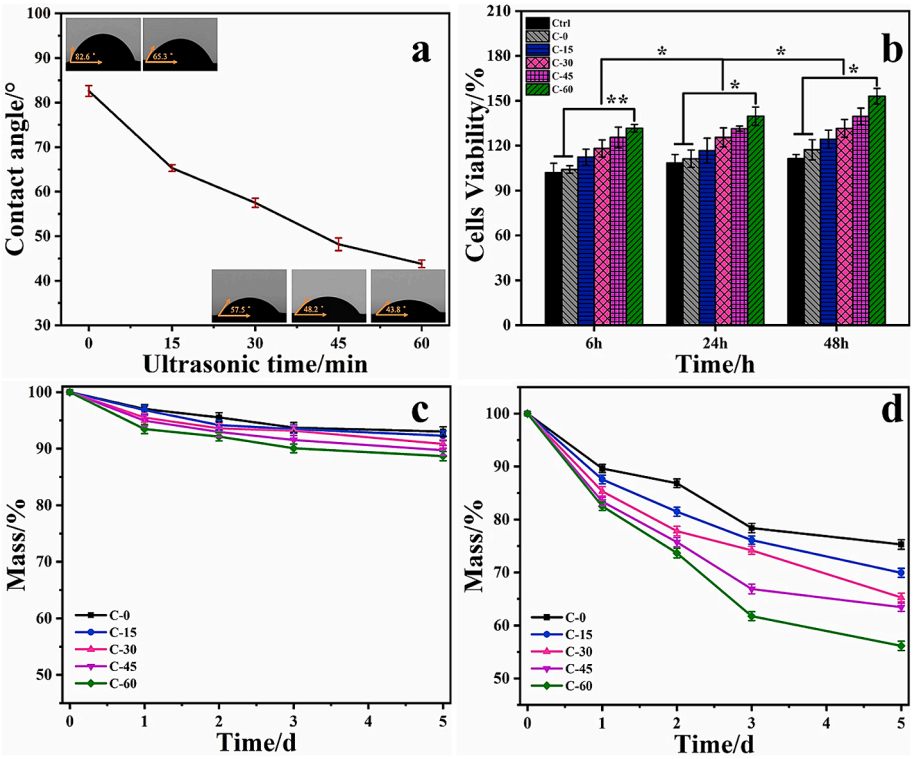

Fig. 6. Water contact angle of tussah silk fiber membrane samples after various durations of ultrasound treatment (a). Viability histograms of mouse fibroblasts (L929) attached to tussah silk fiber membrane samples after 6, 24, and 48 h (b), using a glass surface as a control (*p < 0.05, p < 0.01). Biodegradation profiles of tussah silk fiber samples in PBS buffer (c) and proteinase E solution (d).

and 60 min of treatment (C-45 and C-60), viability rates after 6 h reached 125.51 % and 131.64 %, respectively, showing a notable improvement over the C-15 sample treated briefly with ultrasound (112.36 % survival rate). Ultrasonic treatment can increase the *β*-sheet structure content of SF, which enhances the surface area, stability, and hydrophilicity of the material, providing more contact sites and a more suitable growth environment for cell adhesion. These enhancements confirm the non-cytotoxic and biocompatible nature of the treated tussah silk fiber membranes, which is consistent with findings by Chen *et al.* [75], who reported increased NIH-3 T3 cell proliferation on tussah silk nanofiber mats over time, indicating robust long-term biocompatibility.

Biodegradability is essential for material applications in biomedicine [15,76,77]. The biodegradability of tussah silk materials was examined by immersing samples treated for different ultrasound durations in deionized water, PBS buffer, and proteinase E solution. Extending the ultrasonication time generally enhanced the materials' degradation rates. For instance, degradation rates after 5 days in PBS buffer were 6.98 % (C-0), 7.71 % (C-15), 9.15 % (C-30), 10.28 % (C-45), and 11.33 % (C-60), as shown in Fig. 6c. Similar trends were observed in deionized water, but at slightly lower rates (**Fig. S6**). In proteinase E solution, the enzymatic degradation rates were considerably higher, reflecting protease E's efficacy in breaking down tussah silk proteins, as illustrated in Fig. 6d. The rate of degradation increased with prolonged ultrasonication; for example, it climbed from 10.36 % (C-0) to 17.49 % (C-60) by the first day, reaching a peak of about 43.86 % by the fifth day for C-60. Factors influencing silk material degradation rates include microstructure, molecular weight, and surface morphology [15,73,78,79]. Studies have shown that polar amino acid residues in hydrophilic fragments of silk proteins are more prone to enzymatic attack, while *β*-sheet structures, often hydrophobic, are more resistant to degradation. Arai *et al.* [78] reported that low molecular weight and loosely structured silk proteins are more susceptible to enzymatic breakdown. Additionally, Luo *et al.* [79] observed faster degradation rates for biomaterials with larger pore sizes, though materials with denser pore structures degraded more slowly. Ultrasound treatment not only improved the microscopic morphology of tussah silk fibers but also enhanced their surface hydrophilicity, both of which accelerate the degradation process.

3.6. Mechanism of ultrasound effect on spray-spun tussah silk material

The secondary structure of proteins is not only important for the function of silk material but also a key factor affecting the properties of the biomaterials. Methods to modulate the secondary structure of silk material have been widely investigated, including modulation of temperature, pH, concentration, and ultrasound to control the self-assembly of silk material, or the rearrangement of silk protein molecular chains through solvent treatment, such as water and methanol [18,80]. For example, Li *et al.* [81] demonstrated that conditions such as SF concentration, temperature, and ultrasound can somewhat control the structural properties and conformational transitions of regenerated SF, inducing a significant conformational transition from random coils to *β*-sheets when applying ultrasound to the regenerated SF solution or increasing the SF concentration and temperature.

Based on our experimental results and analyses, we propose a mechanism for the effect of ultrasound treatment on the morphology and structure of tussah silk materials (Fig. 7) to explain the impacts of varying ultrasound durations in ionic liquid-based systems on the thermal, mechanical, and biological properties of spray-spun tussah silk fibrous membranes. Ultrasound plays a synergistic role in ionic liquid systems. During propagation, the interaction between ultrasound and ionic liquid causes cavitation, and ILs produce cavitation bubbles. As ultrasonic duration increases, more cavitation bubbles accumulate sufficient sound energy and collapse (Fig. 7a). In a very brief period, the area around the cavitation bubble reaches high temperatures above 5000 K and high pressures of about 500 atm, generating powerful shock waves and jets [82,83]. This scenario provides a novel and highly

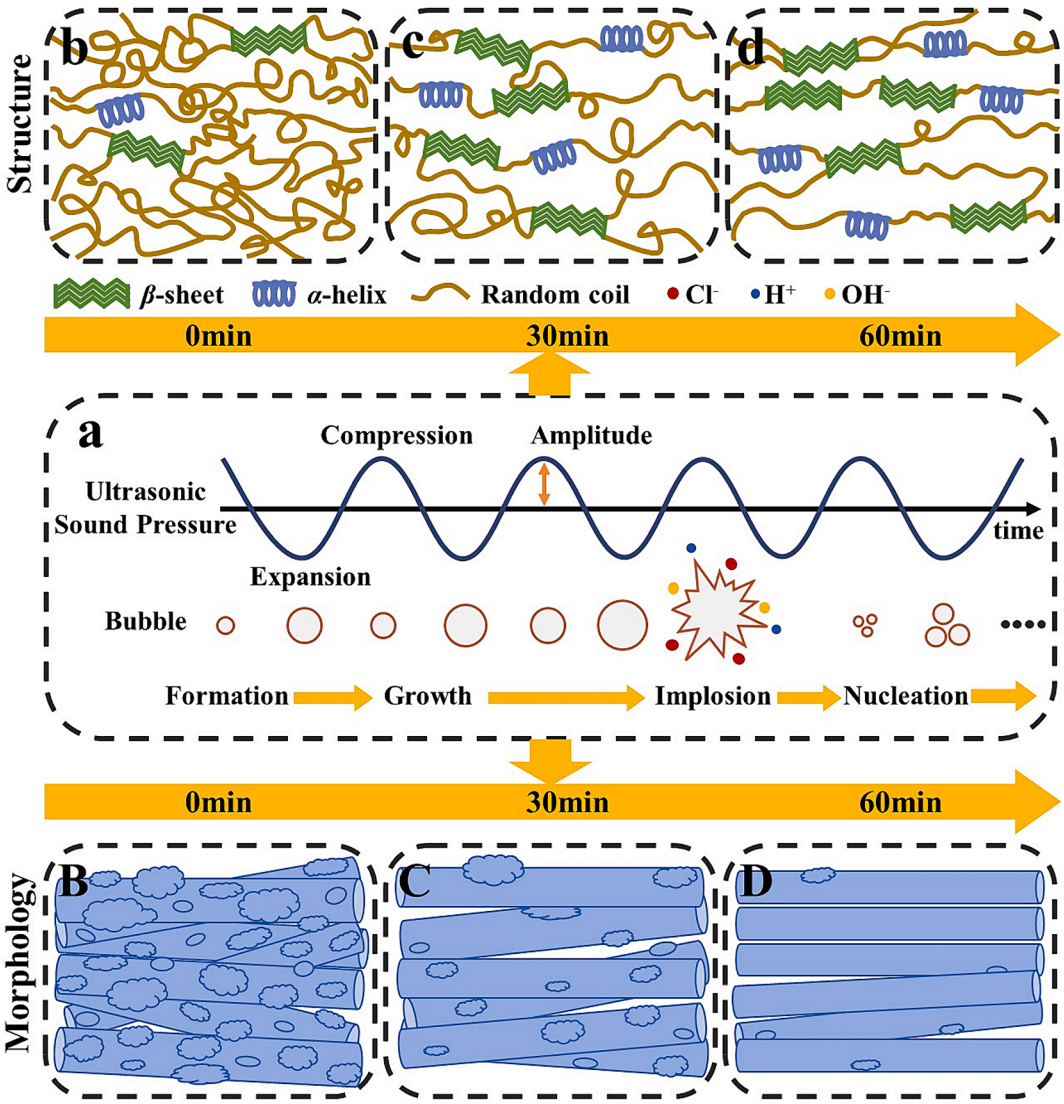

Fig. 7. Mechanism of the effect of ultrasound treatment on the process of spray spinning tussah silk fibers based on an ionic liquid system.

energetic physical environment for the interaction of tussah silk materials, thus accelerating the movement of ionic liquid and TSF macromolecules, intensifying molecular collisions, and enhancing the interaction between ionic liquid and the hydroxyl and amino groups on the tussah silk protein chain to form hydrogen bonds, while weakening or further disrupting the original TSF hydrogen bond network from both external and internal influences [71,81,84]. This effect of ultrasound in ionic liquid is markedly different from its impact in traditional organic solvents, where less efficient cavitation and weaker interactions with molecular structures often lead to suboptimal modification of material properties. In contrast, the enhanced cavitation efficiency and stronger molecular interactions in ionic liquid not only improve the dispersibility and alignment of silk fibroin chains but also lead to more pronounced modifications in mechanical strength and thermal stability.

As illustrated in Fig. 7b, 7c, and 7d, the cascade of molecular-level interactions induces the molecular chain segments of tussah silk to rearrange more orderly, thereby promoting the transformation of the random coil structure into ordered α-helix and β-sheets, which significantly improves the thermal and mechanical properties of tussah silk materials [62,70]. Specifically, long-term ultrasonic treatment increased the β-sheet content from 50.26 % to 54.32 %. These structural changes raised the T_{onset} and T_{pmax} of the material to 256.38 °C and 280.82 °C, respectively. Additionally, the hardness (H) and elastic modulus (E_s) of TSF were also improved. Furthermore, ultrasound also engages in mechanical and thermal interactions with the material, which fosters changes in the shape, structure, and performance of the regenerated TSF. As the regenerated tussah silk solution undergoes flow and tensile forces during the spray spinning process, prolonged ultrasonic treatment breaks down long nanofibers into shorter fibers, reducing viscosity and enhancing the rheology of the spray spinning solution [47,48,85]. The viscosity decreased from approximately 0.4 Pa·s for the untreated sample to about 0.2 Pa·s after 60 min of ultrasonic treatment. Simultaneously, the high temperature and pressure generated by ultrasonic cavitation also promote the dissolution and dispersion of tussah silk [27,82]. These factors improve the stability of the jet stream and promote the formation of fibers with smaller diameters, more uniform thickness, and smoother surfaces (Fig. 7B, 7C, and 7D) [46,85,86]. Previous studies [30,56,57] corroborate our findings; for instance, Cai *et al.* [56] showed that increasing ultrasound duration or power could enhance the self-assembly of silk molecules, forming more β-sheet structures and improving the material's physical properties, such as thermal stability. Ultrasonic treatment also ensures that more hydrophilic groups are evenly distributed on the surface of the material, thereby improving the hydrophilicity of the sample [57,87,88]. This enhancement facilitates cell adhesion and proliferation and improves the material's biocompatibility. The results from FTIR, XRD, and

thermal analysis experiments also support this hypothesis.

In conclusion, our experimental findings suggest that increasing the ultrasound treatment duration in AMIMCl solution promotes changes in the protein structure of tussah silk and enhances the thermal, mechanical, and biological properties of tussah silk materials.

4. Conclusion

In this work, we propose a method for preparing wild tussah silk fiber membranes using a combination of ultrasound treatment and solution jet spinning techniques in an ionic liquid system. We investigated the effects of various ultrasound treatment durations on the morphology, structure, and properties of tussah silk fiber samples. Through SEM analysis, it was observed that ultrasound treatment could reduce the viscosity of the solution, which affects the stretching of the jet-spun solution to form fibers. FTIR and XRD analyses confirmed that increasing the ultrasound treatment duration enhances the hydrogen bonding interactions between the protein chains of tussah silk, promotes the transition from random coils to ordered β-sheets and α-helices, and improves the crystallinity of the material. These structural changes further influence the thermal and mechanical properties of the material. For example, as ultrasound time increased from 0 to 60 min, the content of β-sheet structures in the sample significantly increased to 54.32 %. Correspondingly, the temperature of maximum weight loss rate (T_{pmax}) and the elastic modulus (E_s) increased by 12.57 °C and 0.2 GPa, respectively. Additionally, the biological properties of the tussah silk material were evaluated through water contact angle measurements, cell proliferation experiments, and enzymatic degradation tests. The results showed that longer ultrasound treatment times increased the hydrophilicity and enzymatic degradation rate of the material, enhancing the conditions conducive to cell growth and proliferation on the surface of tussah silk materials, thus improving their biocompatibility. Based on these findings, we propose a molecular model to elucidate the effects of ultrasound treatment on the morphology, structure, and properties of tussah silk materials.

This study successfully demonstrates that the structure and properties of protein fiber materials can be flexibly modulated through ultrasound technology in biocompatible ionic liquids, which is crucial for developing natural biomaterials that meet the needs of biomedical and tissue engineering applications. This method not only offers a novel and efficient preparation technique but also provides valuable insights for further research into the high-performance and multifunctional applications of tussah silk materials, aiding in the achievement of sustainable development goals (SDGs).

CRediT authorship contribution statement

Xincheng Zhuang: Writing – original draft, Investigation, Formal analysis, Data curation. **Haomiao Zhu:** Data curation. **Fang Wang:** Writing – review & editing, Writing – original draft, Supervision, Funding acquisition, Conceptualization. **Xiao Hu:** Writing – review & editing, Funding acquisition, Conceptualization.

Declaration of competing interest

The authors declare that they have no known competing financial interests or personal relationships that could have appeared to influence the work reported in this paper.

Data availability

Data will be made available on request.

Acknowledgements

This study is supported by the National Natural Science Foundation of China (21973045). X.H. is supported by Rowan University Seed Research Grants, and the US NSF Future Manufacturing Program (CMMI-2037097).

Appendix A. Supplementary data

Supplementary data to this article can be found online at https://doi.org/10.1016/j.ultsonch.2024.107018.

References

[1] E. Kabir, R. Kaur, J. Lee, K.H. Kim, E.E. Kwon, Prospects of biopolymer technology as an alternative option for non-degradable plastics and sustainable management of plastic wastes, J. Clean. Prod. 258 (2020) 120536.
[2] A.Z. Naser, I. Deiab, B.M. Darras, Poly (lactic acid)(PLA) and polyhydroxyalkanoates (PHAs), green alternatives to petroleum-based plastics: A review, RSC Adv. 11 (2021) 17151–17196.
[3] F. Yang, J. Dian, Macro-economic impact of policies for controlling fossil energy consumption in China, Energies 15 (2022) 1051.
[4] H. Liu, R. Jian, H. Chen, X. Tian, C. Sun, J. Zhu, Z. Yang, J. Sun, C. Wang, Application of biodegradable and biocompatible nanocomposites in electronics: Current status and future directions, Nanomaterials 9 (2019) 950.
[5] X. Zhuang, F. Wang, X. Hu, Biodegradable polymers: A promising solution for green energy devices, Eur. Polym. J. 112696 (2023).
[6] Y. Huang, S. Kormakov, X. He, X. Gao, X. Zheng, Y. Liu, J. Sun, D. Wu, Conductive polymer composites from renewable resources: an overview of preparation, properties, and applications, Polymers 11 (2019) 187.
[7] S. Bhatia, Natural polymers vs synthetic polymer, Natural polymer drug delivery systems: nanoparticles, plants, and algae, (2016) 95-118.
[8] N. Gowthaman, H. Lim, T. Sreeraj, A. Amalraj, S. Gopi, Advantages of biopolymers over synthetic polymers: Social, economic, and environmental aspects, in: Biopolymers and Their Industrial Applications, Elsevier, 2021, pp. 351–372.
[9] R. Mohammadinejad, A. Kumar, M. Ranjbar-Mohammadi, M. Ashrafizadeh, S. S. Han, G. Khang, Z. Roveimiab, Recent advances in natural gum-based biomaterials for tissue engineering and regenerative medicine: A review, Polymers 12 (2020) 176.
[10] Y. Xue, D. Jao, W. Hu, X. Hu, Silk-silk blend materials: A comparative study of Mori-Tussah, Mori-Muga, Mori-Eri, and Mori-Thai silk films, J. Therm. Anal. Calorim. 127 (2017) 915–921.
[11] M.B. Üzümcü, İ. Borazan, M. Kaplan, Wild silk fibers: Types, properties and utilization areas, (2019).
[12] B. Kundu, R. Rajkhowa, S.C. Kundu, X. Wang, Silk fibroin biomaterials for tissue regenerations, Adv. Drug Deliv. Rev. 65 (2013) 457–470.
[13] Z. Wang, H. Yang, W. Li, C. Li, Effect of silk degumming on the structure and properties of silk fibroin, J. Text. Inst. 110 (2019) 134–140.
[14] M. Zhao, Z. Qi, X. Tao, C. Newkirk, X. Hu, S. Lu, Chemical, thermal, time, and enzymatic stability of silk materials with silk i structure, Int. J. Mol. Sci. 22 (2021) 4136.
[15] S. Zou, X. Yao, H. Shao, R.L. Reis, S.C. Kundu, Y. Zhang, Nonmulberry silk fibroin-based biomaterials: Impact on cell behavior regulation and tissue regeneration, Acta Biomater. (2022).
[16] S.S. Silva, B. Kundu, S. Lu, R.L. Reis, S.C. Kundu, Chinese oak tasar silkworm Antheraea pernyi silk proteins: current strategies and future perspectives for biomedical applications, Macromol. Biosci. 19 (2019) 1800252.
[17] Y. Chen, M. Chen, Y. Gao, F. Zhang, M. Jin, S. Lu, M. Han, Biological efficacy comparison of natural tussah silk and mulberry silk nanofiber membranes for guided bone regeneration, ACS Omega 7 (2022) 19979–19987.
[18] H.Y. Wang, Y.Q. Zhang, Z.G. Wei, Dissolution and processing of silk fibroin for materials science, Crit. Rev. Biotechnol. 41 (2021) 406–424.
[19] H.Y. Wang, Y.Q. Zhang, Processing silk hydrogel and its applications in biomedical materials, Biotechnol. Prog. 31 (2015) 630–640.
[20] H.Y. Wang, Z.G. Wei, Y.Q. Zhang, Dissolution and regeneration of silk from silkworm Bombyx mori in ionic liquids and its application to medical biomaterials, Int. J. Biol. Macromol. 143 (2020) 594–601.
[21] M. Kosmulski, J. Gustafsson, J.B. Rosenholm, Thermal stability of low temperature ionic liquids revisited, Thermochim. Acta 412 (2004) 47–53.
[22] E. Judy, N. Kishore, Prevention of insulin fibrillation by biocompatible choline-amino acid based ionic liquids: Biophysical insights, Biochimie 207 (2023) 20–32.
[23] O.A. El Seoud, A. Koschella, L.C. Fidale, S. Dorn, T. Heinze, Applications of ionic liquids in carbohydrate chemistry: a window of opportunities, Biomacromolecules 8 (2007) 2629–2647.
[24] A. Benedetto, P. Ballone, Room temperature ionic liquids meet biomolecules: a microscopic view of structure and dynamics, ACS Sustain. Chem. Eng. 4 (2016) 392–412.
[25] D. Dehnad, S.M. Jafari, M. Afrasiabi, Influence of drying on functional properties of food biopolymers: From traditional to novel dehydration techniques, Trends Food Sci. Technol. 57 (2016) 116–131.
[26] X. Wang, M. Majzoobi, A. Farahnaky, Ultrasound-assisted modification of functional properties and biological activity of biopolymers: A review, Ultrason. Sonochem. 65 (2020) 105057.
[27] W. Wang, H. Long, L. Chen, Y. Liu, Q. Li, Ultrasonics induced variations in molecular structure and tensile properties of silk fibers in a chemical free environment, Nano Select 2 (2021) 1962–1967.

[28] Y.W. Cho, Y.N. Cho, S.H. Chung, G. Yoo, S.W. Ko, Water-soluble chitin as a wound healing accelerator, Biomaterials 20 (1999) 2139–2145.
[29] A. Aluigi, C. Vineis, A. Ceria, C. Tonin, Composite biomaterials from fibre wastes: Characterization of wool–cellulose acetate blends, Compos. A Appl. Sci. Manuf. 39 (2008) 126–132.
[30] F. Yang, F. Wang, J. Mazahreh, X. Hu, Ultrasound-assisted air-jet spinning of silk fibroin-soy protein nanofiber composite biomaterials, Ultrason. Sonochem. 94 (2023) 106341.
[31] X. Wang, Z. Yu, Y. Zhang, C. Qi, W.-L. Chang, Evaluation of ultrasonic-assisted dyeing properties of fast-growing poplar wood treated by reactive dye based on grey system theory analysis, J. Wood Sci. 64 (2018) 861–871.
[32] H.J. Jin, D.L. Kaplan, Mechanism of silk processing in insects and spiders, Nature 424 (2003) 1057–1061.
[33] Y. Sun, M. Zhang, D. Fan, Effect of ultrasonic on deterioration of oil in microwave vacuum frying and prediction of frying oil quality based on low field nuclear magnetic resonance (LF-NMR), Ultrason. Sonochem. 51 (2019) 77–89.
[34] L. Rayleigh VIII, On the pressure developed in a liquid during the collapse of a spherical cavity, London Edinburgh Dublin Philosoph. Mag. J. Sci. 34 (1917) 94–98.
[35] T.S. Leong, G.J. Martin, M. Ashokkumar, Ultrasonic encapsulation–A review, Ultrason. Sonochem. 35 (2017) 605–614.
[36] S. Merouani, O. Hamdaoui, Y. Rezgui, M. Guemini, Energy analysis during acoustic bubble oscillations: Relationship between bubble energy and sonochemical parameters, Ultrasonics 54 (2014) 227–232.
[37] W.C. Oliver, G.M. Pharr, An improved technique for determining hardness and elastic modulus using load and displacement sensing indentation experiments, J. Mater. Res. 7 (1992) 1564–1583.
[38] H. Cho, A. Shakil, A.A. Polycarpou, S. Kim, Enabling selectively tunable mechanical properties of graphene oxide/silk fibroin/cellulose nanocrystal bionanofilms, ACS Nano 15 (2021) 19546–19558.
[39] M. Wang, H.-J. Jin, D.L. Kaplan, G.C. Rutledge, Mechanical properties of electrospun silk fibers, Macromolecules 37 (2004) 6856–6864.
[40] F. Wang, S.J. Aravind, H. Wu, J. Forys, V. Venkataraman, K. Ramanujachary, X. Hu, Tunable green graphene-silk biomaterials: Mechanism of protein-based nanocomposites, Mater. Sci. Eng. C 79 (2017) 728–739.
[41] K. Zhang, F. Si, H. Duan, J. Wang, Microstructures and mechanical properties of silks of silkworm and honeybee, Acta Biomater. 6 (2010) 2165–2171.
[42] S. Park, K.P. Marimuthu, G. Han, H. Lee, Deep learning based nanoindentation method for evaluating mechanical properties of polymers, Int. J. Mech. Sci. 246 (2023) 108162.
[43] G. Qin, S. Lapidot, K. Numata, X. Hu, S. Meirovitch, M. Dekel, I. Podoler, O. Shoseyov, D.L. Kaplan, Expression, cross-linking, and characterization of recombinant chitin binding resilin, Biomacromolecules 10 (2009) 3227–3234.
[44] C. Wang, C. Liang, R. Wang, X. Yao, P. Guo, W. Yuan, Y. Liu, Y. Song, Z. Li, X. Xie, The fabrication of a highly efficient self-healing hydrogel from natural biopolymers loaded with exosomes for the synergistic promotion of severe wound healing, Biomater. Sci. 8 (2020) 313–324.
[45] M.P. Ho, H. Wang, K.T. Lau, Effect of degumming time on silkworm silk fibre for biodegradable polymer composites, Appl. Surf. Sci. 258 (2012) 3948–3955.
[46] J. He, Y. Qin, S. Cui, Y. Gao, S. Wang, Structure and properties of novel electrospun tussah silk fibroin/poly (lactic acid) composite nanofibers, J. Mater. Sci. 46 (2011) 2938–2946.
[47] Y. Iida, T. Tuziuti, K. Yasui, A. Towata, T. Kozuka, Control of viscosity in starch and polysaccharide solutions with ultrasound after gelatinization, Innov. Food Sci. Emerg. Technol. 9 (2008) 140–146.
[48] J.Z. Wang, X.B. Huang, J. Xiao, N. Li, W.T. Yu, W. Wang, W.Y. Xie, X.J. Ma, Y. L. Teng, Spray-spinning: a novel method for making alginate/chitosan fibrous scaffold, J. Mater. Sci. - Mater. Med. 21 (2010) 497–506.
[49] N. Wang, L. Wu, J. Yang, Y. You, F. Zhang, J. Kan, J. Zheng, Lotus starch/bamboo shoot polysaccharide composite system treated via ultrasound: Pasting, gelling properties and multiscale structure, Food Res. Int. 174 (2023) 113605.
[50] K. Li, W. Xue, S. Hua, Study on process optimization and wetting performance of ultrasonic-oxidized wool fiber, Autex Res. J. (2022).
[51] Y. Li, J. Wang, Y. Wang, W. Cui, Advanced electrospun hydrogel fibers for wound healing, Compos. B Eng. 223 (2021) 109101.
[52] N. Drnovšek, R. Kocen, A. Gantar, M. Drobnič Košorok, A. Leonardi, I. Križaj, A. Rečnik, S. Novak, Size of silk fibroin β-sheet domains affected by Ca^{2+}, J. Mater. Chem. B 4 (2016) 6597–6608.
[53] K. Križman, S. Novak, J. Kristl, G. Majdič, N. Drnovšek, Long-acting silk fibroin xerogel delivery systems for controlled release of estradiol, J. Drug Deliv. Sci. Technol. 65 (2021) 102701.
[54] K.G. Hausken, R.L. Frevol, K.P. Dowdle, A.N. Young, J.M. Talusig, C.C. Holbrook, B.K. Rubin, A.R. Murphy, Quantitative functionalization of the tyrosine residues in silk fibroin through an amino-tyrosine intermediate, Macromol. Chem. Phys. 223 (2022) 2200119.
[55] X. Hu, D. Kaplan, P. Cebe, Determining beta-sheet crystallinity in fibrous proteins by thermal analysis and infrared spectroscopy, Macromolecules 39 (2006) 6161–6170.
[56] B. Cai, H. Gu, F. Wang, K. Printon, Z. Gu, X. Hu, Ultrasound regulated flexible protein materials: Fabrication, structure and physical-biological properties, Ultrason. Sonochem. 79 (2021) 105800.
[57] F. Yang, B. Cai, H. Gu, F. Wang, Comparative investigation on the structure and properties of protein films from domestic and wild silkworms through ultrasonic regeneration, J. Mol. Struct. 1283 (2023) 135255.
[58] N. Goujon, R. Rajkhowa, X. Wang, N. Byrne, Effect of solvent on ionic liquid dissolved regenerated antheraea assamensis silk fibroin, J. Appl. Polym. Sci. 128 (2013) 4411–4416.
[59] A. Reizabal, C. Costa, P. Saiz, B. Gonzalez, L. Pérez-Álvarez, R.F. de Luis, A. Garcia, J. Vilas Vilela, S. Lanceros Méndez, Processing strategies to obtain highly porous silk fibroin structures with tailored microstructure and molecular characteristics and their applicability in water remediation, J. Hazard. Mater. 403 (2021) 123675.
[60] F. Zhang, B.Q. Zuo, H.X. Zhang, L. Bai, Studies of electrospun regenerated SF/TSF nanofibers, Polymer 50 (2009) 279–285.
[61] Y. Xue, F. Wang, M. Torculas, S. Lofland, X. Hu, Formic acid regenerated mori, tussah, eri, thai, and muga silk materials: Mechanism of self-assembly, ACS Biomater Sci. Eng. 5 (2019) 6361–6373.
[62] Y.Y. Wang, Y.D. Cheng, Y. Liu, H.J. Zhao, M.Z. Li, The effect of ultrasonication on the gelation velocity and structure of silk fibroin, Adv. Mat. Res. 175 (2011) 143–148.
[63] F. Yang, B. Cai, H. Heng, H. Gu, F. Wang, Preparation, structure and properties of soy protein and silk fibroin composite nanofiber membrane by jet spinning, Sci. Sin. Chim. 52 (2022) 709–720.
[64] D.C. Kong, M.H. Yang, X.S. Zhang, Z.C. Du, Q. Fu, X.Q. Gao, J.W. Gong, Control of polymer properties by entanglement: a review, Macromol. Mater. Eng. 306 (2021) 2100536.
[65] S. He, J. Zhang, X. Xiao, X. Hong, Effects of ultrasound vibration on the structure and properties of polypropylene/graphene nanoplatelets composites, Polym. Eng. Sci. 58 (2018) 377–386.
[66] R. Yang, P. Wu, X. Wang, Z. Liu, C. Zhang, Y. Shi, F. Zhang, B. Zuo, A novel method to prepare tussah/Bombyx mori silk fibroin-based films, RSC Adv. 8 (2018) 22069–22077.
[67] J.B. Park, Biomaterials Science and Engineering, Springer Science & Business Media, 2012.
[68] X. Hu, X. Wang, J. Rnjak, A.S. Weiss, D.L. Kaplan, Biomaterials derived from silk–tropoelastin protein systems, Biomaterials 31 (2010) 8121–8131.
[69] R. Serôdio, S.L. Schickert, A.R. Costa-Pinto, J.R. Dias, P.L. Granja, F. Yang, A. L. Oliveira, Ultrasound sonication prior to electrospinning tailors silk fibroin/PEO membranes for periodontal regeneration, Mater. Sci. Eng. C 98 (2019) 969–981.
[70] B. Cai, J. Mazahreh, Q. Ma, F. Wang, X. Hu, Ultrasound-assisted fabrication of biopolymer materials: A review, Int. J. Biol. Macromol. 209 (2022) 1613–1628.
[71] H.Y. Wang, Y.Y. Chen, Y.Q. Zhang, Processing and characterization of powdered silk micro-and nanofibers by ultrasonication, Mater. Sci. Eng. C 48 (2015) 444–452.
[72] A. Sakai, Y. Murayama, K. Fujiwara, T. Fujisawa, S. Sasaki, S. Kidoaki, M. Yanagisawa, Increasing elasticity through changes in the secondary structure of gelatin by gelation in a microsized lipid space, ACS Cent. Sci. 4 (2018) 477–483.
[73] H. Gu, F. Wang, H. Liu, K. Printon, X. Hu, Multifunctional silk fibroin–Poly (L-lactic acid) porous nanofibers: Designing adjustable nanopores to control composite properties and biological responses, Mater. Des. 222 (2022) 111053.
[74] J. Wang, Y. Chen, G. Zhou, Y. Chen, C. Mao, M. Yang, Polydopamine-coated Antheraea Pernyi (a. Pernyi) silk fibroin films promote cell adhesion and wound healing in skin tissue repair, ACS Appl. Mater. Interfaces 11 (2019) 34736–34743.
[75] M. Chen, J. Qin, S. Lu, F. Zhang, B. Zuo, Robust nanofiber mats exfoliated from tussah silk for potential biomedical applications, Front. Bioeng. Biotechnol. 9 (2021) 746016.
[76] H. Zhang, R. You, K. Yan, Z. Lu, Q. Fan, X. Li, D. Wang, Silk as templates for hydroxyapatite biomineralization: A comparative study of Bombyx mori and Antheraea pernyi silkworm silks, Int. J. Biol. Macromol. 164 (2020) 2842–2850.
[77] C. Lujerdean, G.M. Baci, A.A. Cucu, D.S. Dezmirean, The contribution of silk fibroin in biomedical engineering, Insects 13 (2022) 286.
[78] T. Arai, G. Freddi, R. Innocenti, M. Tsukada, Biodegradation of Bombyx mori silk fibroin fibers and films, J. Appl. Polym. Sci. 91 (2004) 2383–2390.
[79] Z. Luo, Q. Zhang, M. Shi, Y. Zhang, W. Tao, M. Li, Effect of pore size on the biodegradation rate of silk fibroin scaffolds, Adv. Mater. Sci. Eng. 2015 (2015).
[80] J. Zhou, B. Zhang, L. Shi, J. Zhong, J. Zhu, J. Yan, P. Wang, C. Cao, D. He, Regenerated silk fibroin films with controllable nanostructure size and secondary structure for drug delivery, ACS Appl. Mater. Interfaces 6 (2014) 21813–21821.
[81] X.G. Li, L.Y. Wu, M.R. Huang, H.L. Shao, X.C. Hu, Conformational transition and liquid crystalline state of regenerated silk fibroin in water, Biopolymers: Original Research on, Biomolecules 89 (2008) 497–505.
[82] X. Sun, S. Liu, X. Zhang, Y. Tao, G. Boczkaj, J.Y. Yoon, X. Xuan, Recent advances in hydrodynamic cavitation-based pretreatments of lignocellulosic biomass for valorization, Bioresour. Technol. 345 (2022) 126251.
[83] T. Truong Dinh Tran, P. Ha Lien Tran, K. Tu Nguyen, V.T. Tran, Nano-precipitation: preparation and application in the field of pharmacy, Curr. Pharm. Des. 22 (2016) 2997–3006.
[84] L. Huang, J. Shi, W. Zhou, Q. Zhang, Advances in $, Int. J. Mol. Sci. 24 (2023) 13153.
[85] D. Yao, T. Wang, X. Zhang, Y. Wang, High concentration crystalline silk fibroin solution for silk-based materials, Materials 15 (2022) 6930.
[86] Q. Cao, Y. Wan, J. Qiang, R. Yang, J. Fu, H. Wang, W. Gao, F. Ko, Effect of sonication treatment on electrospinnability of high-viscosity PAN solution and mechanical performance of microfiber mat, Iran. Polym. J. 23 (2014) 947–953.
[87] S. Zhou, Y. Li, L. Huang, L. Chen, Y. Ni, Q. Miao, Ultrasonic treatment for enhancing the accessibility and reactivity of softwood rayon-grade kraft-based dissolving pulp, Cellul. 26 (2019) 9287–9294.
[88] H. He, Z. Zhang, Z. Qi, Y. Jiang, M. Zuo, H. Zuo, Q. Chen, Z. Cheng, P. Li, High-Frequency Ultrasonic Assisted Natural Silk Fibroin: A Polycyclic Aromatic Hydrocarbons Scavenger, Sci. Adv. Mater. 11 (2019) 1531–1536.